PAPER

Preparation of SiO$_2$ resin coating with superhydrophobic wettability and anti-icing behavior analysis

Xiaoru Hao, [iD] *[a] Jun Xie,[a] Yu Zhang,[a] Zhihao Cheng[a] and Wei Sheng[ab]

Among different types of anti-icing coatings, superhydrophobic surfaces have attracted extensive attention due to their excellent water repellency and low thermal conductivity. We report facile spraying time tuning to optimize the superhydrophobic (SHP) surface coating fabrication by a one-step spraying method of mixing SiO$_2$ nanoparticles with epoxy resin (EP), polyamide resin (PAI), and HFTMS. The wettability performance was optimized by adjusting spraying time from 0 s to 25 s to control surface morphology by adjusting surface morphology and line roughness. With spraying time of 20 s, SiO$_2$ molecular clusters on the superhydrophobic surface showed a maximum water contact angle (WCA) of 160.4° ± 1.3° and a sliding angle (SA) of 4.1° ± 1.0°. What's more, the effect of the coatings' icing behavior were studied by icing heat conduction; SHP-20 delayed the icing time for 410 s at −15 °C, and the icing performance of SHP-20 also declined with the decrease of temperature to −9 °C, −12 °C, −15 °C, and −18 °C. The WCA of SHP-20 can remain above 140.9° ± 1.8° after 40 abrasive 1000# sandpaper wear cycles. The results also provide a basis for the preparation of SHP and anti-icing characteristics.

Introduction

Inspired by the special properties of natural biological surfaces including lotus leaf surfaces and butterfly wings, super-hydrophobic (SHP) surfaces have applications in many emerging industries, including anti-icing,[1] self-cleaning,[2] fluid rent reduction,[3] *etc.* In the application of metal materials, the hydrophilicity of their surfaces often leads to material failure. HFTMS as a known and lowest surface energy modifier yet recorded (6.7 mJ m^{-2} was attained for a surface with regularly aligned closest-hexagonal packed –CF$_3$ groups) has been proved to be able to react with hydrophilic –OH group to form hydrophobic groups with low surface energy.[4,5] At the same time, it can also enhance the bonding ability between metal matrix and organic coating.[6,7] SiO$_2$ nanoparticles are a hydrophilic and attractive material for superhydrophobic coatings which have –OH group on the surface due to cheaper,[8] chemically stable,[9] harmless, and low thermal conductivity.[10] Thus, we can modify SiO$_2$ molecules to obtain a stable superhydrophobic coating and study its reaction mechanism.

The surface with water contact angle more than 150° can be realized by adjusting the surface structure and surface energy.[11] Currently, a large number of superhydrophobic materials have been prepared on different substrates by chemical electro-spinning,[12] laser etching,[13–15] electrochemical treatment,[16,17]

physical or chemical deposition,[18,19] and self-assembly[20,21] to get superhydrophobic wettability. T. P. Manoj *et al.*[22] fabricated a superhydrophobic surface by changing the etching time of titanium alloy in acid, the coating exhibits a maximum WCA of 162.3° ± 1° with a sliding angle of 1°. A. Gaddam *et al.*[23] studied one step femtosecond laser processing to get single-tier nano and two-tier multiscale structure to learn more about the surface morphology and surface hydrophobicity, and the experimental results show that the multi-scale surface morphology features have good hydrophobicity. However, most of these methods require fine technology and damage of surface metal characteristics that cannot achieve large-scale production. In addition, many researchers obtain superhydrophobic surfaces by changing the surface energy parameters of coatings.[24,25] The coating prepared by spraying can be applied to most alloys and has low thermal conductivity, and spraying low surface energy substances on the surface can effectively obtain appropriate surface roughness that the surface has superhydrophobic properties economically. W. Guo[26] prepared a superhydrophobic surface with fluorinated epoxy and unmodified-nano SiO$_2$ and micron SiO$_2$, the contact angle for water was 158.6° ± 1°. However, the anti-icing performance of the coatings has not been satisfactorily achieved. As a result, most superhydrophobic surfaces can be ideal candidates for anti-icing surfaces,[27,28] the micro–nano structure design and water-repellent properties of coatings have a great influence on the icing performance of droplets on the coating surface.[29,30] Further, delaying the freezing process of droplets mechanism with an incomplete description and understanding and the

[a]School of Mechanical and Power Engineering, Henan Polytechnic University, Jiaozuo, 454003, P. R. China. E-mail: xiaoru408@126.com

[b]Hami Yuxin New Energy Industry Research Institute, Hami, 839000, P. R. China

function of superhydrophobic coatings icing behaviors under different temperature which also limits its practical application.

In this paper, we report a simple, economical preparation method by coatings in which the EP, PAI, and HFTMS were self-assembled onto SiO_2 particles, and study the reaction process. Experiment was designed as a one-step spraying method to get superhydrophobic coating (SHP) that studied the surface morphology of spraying time with 0 s to 25 s. The icing behaviors of SHP surfaces were optimized at −15 °C, and coatings with the best hydrophobicity were studied at the different temperature of −9 °C, −12 °C, −15 °C, and −18 °C through the self-made anti-icing experimental process. And the durability and mechanical properties of the surface with the best hydrophobicity were tested.

Experimental

Materials

7075 aluminum alloy (40 mm × 40 mm × 2 mm), purchased from Shenzhen Shengjili Co., Ltd; trimethoxy (1H,1H,2H,2H-heptafluorodecyl, HFTMS) silane, purchased from Aladdin Reagent Co., Ltd; gas-phase nano-silica SiO_2 (hydrophilicity, particle size about 20 nm), purchased from Zhiding Welding Materials Co., Ltd; epoxy resin (EP, 40 000–50 000 Pa s/25 °C), polyamide resin (PAI, 12 000–25 000 mPa s/40 °C), purchased from Zhejiang Jinhong Co., Ltd; ethanol (CH_3CH_2OH) and acetone (CH_3COCH_3) were purchased from Sinopharm Chemical Reagent Co., Ltd.

Sample preparation

7075 aluminum alloy (40 mm × 40 mm × 2 mm) is polished 800#, 1000#, and 2000# emery papers to refine the surface roughness and machining tool marks of the aluminum plate, subsequently, it was polished by a P-2 metallographic sample polishing machine to remove the alumina film on the surface of aluminum plate. Then, it was placed in acetone solution at room temperature, ultrasonic cleaning, and ethanol solution for 10 min. These steps are mainly used for various oil stains on the sample surface to reduce the influence of the oil film on the subsequent experiments. 1 g SiO_2 nanoparticles were dispersed in 20 ml ethanol and treated by ultrasonic dispersion for 30 min. Subsequently, 2 ml a mass fraction of 1% HFTMS ethanol solution was added to the SiO_2/ethanol dispersion, and the HFTMS was hydrolyzed and self-assembled into SiO_2 nanoparticles. Then, the modified SiO_2 epoxy dispersion was obtained by adding 0.5 g EP and 0.5 g PAI modified SiO_2 nanoparticles. What's more, to investigate the effect of applied potential on superhydrophobic, the pre-cured modified SiO_2 epoxy dispersion is sprayed on the cleaned aluminum substrate as an adhesive layer. And spraying time in different duration ranging from 0 s to 25 s to investigate the performance of the coating surface. The air pressure of the spray gun is set to 30 psi, and the distance between the spray nozzle and the base plate and the diameter of the nozzle is 25 cm and 0.13 cm respectively. After spraying, the coating was dried in a hot air oven for 1 h at 80 °C.

Characterization

Merlin compact scanning electron microscope (SEM, Carl Zeiss NTS GmbH, Germany) was used to observe the surface micro-morphology of the sample. To further analyze the surface morphology and structure of the composite coating, the surface micromorphology and bulge height profile of the composite coating were characterized by Ultra-Depth 3D Microscope (VHX-2000, Japan), the surfaces roughness of SHP were tested by SJ-210 (Mitutoyo, Japan).

SDC-350 optical contact angle measuring instrument (Dongguan Sheng Precision Instrument Co., Ltd.) was used to observe the sample surface with a volume of 5 μL water droplets to measure the water contact angle and sliding angle of the sample surfaces by nine water droplets. The final measurement value was calculated by the average value of nine measurements.

Fourier transform infrared spectrometer (FTIR, Bucks HP9 2FX, PerkinElmer, USA) was used to analyze the surface of unmodified and modified nano-silica, and the surface bond energy absorption peaks were analyzed respectively to judge whether fluorinated was hydrolyzed and self-assembled into SiO_2 particles.

The self-made anti-icing experimental device is shown in Fig. 1, which is used to test the anti-icing performance of the SHP surface. The anti-icing experimental device was a visual platform built on the contact angle measurement system device, and mainly completes semiconductor refrigeration functions and real-time image acquisition functions of water droplets. The refrigeration system composes a power supply device, semiconductor refrigeration table, temperature sensor, and water circulation equipment. The anti-performance of SHP was tested by recording the freezing time on it. Here, the experiment was repeated three times and the process of droplets icing was recorded.

The durability of the SHP was evaluated by exposing to the air for 180 days. And the wear resistance of the coating was evaluated by a linear friction test. The experimental steps were as follows. The prepared superhydrophobic coating on the surface of 40 mm × 40 mm × 2 mm aluminum alloy plate was placed side down on 1000# sandpaper with a mass of 200 g above the sample, then moved 10 cm on the sandpaper.
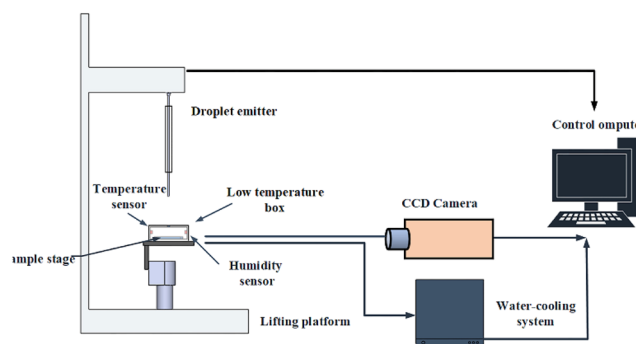

Fig. 1 Self-made anti-icing test bench for superhydrophobic surface.

Recording each reciprocating motion water contact angle and sliding angle every 10 times.

Results and discussion

Analysis of modification mechanism of fluorinated SiO_2 particles

Fig. 2(a) shows the formation mechanism of superhydrophobic coating on fluorinated SiO_2 surface. The reaction is composed of HFTMS and SiO_2 nanoparticles. HFTMS is composed of 5-CF_2- (surface energy of 18 mJ m^{-2}) and 1-CF_3 (the surface energy is 6.7 mJ m^{-2}),[5] this is the lowest surface energy of water repellent. During the reaction, its fluorinated group Si–OC_2H_5 will react to produce silanol Si–OH. $C_{13}H_{13}F_{17}O_3Si$ molecules would shrink with each other to form a covalent bond connection, and a low surface free energy hydrophobic group film can be effectively formed on the microstructure surface. As a result, HFTMS ($C_{13}H_{13}F_{17}O_3Si$) is mixed with it to obtain nanomaterials with a hydrophobic surface. In the process of low surface energy treatment, fluorinated treatment will not affect the surface morphology of SiO_2 particles. Fig. 2(b) shows the FTIR spectrum of fluorinated modified SiO_2. It can be seen in Fig. 2(b) that the absorption peaks at 1073 cm^{-1} and 472 cm^{-1} belong to the characteristic absorption band of Si–O–Si. After

fluorination modification, the peak of –OH at 2851 cm^{-1} and 2935 cm^{-1} of SiO_2 nanoparticles disappeared, the characteristic absorption peak of the –CF_2 bond appears near 1144 cm^{-1}, the characteristic absorption peak of C–F exists near 1243 cm^{-1}, and the epoxy group absorption peaks of epoxy resin and polyamine resin are at 937 cm^{-1} and the peak of 1730 cm^{-1} were the stretching vibration peaks of C=O.[32] Therefore, it can be concluded that the low surface free energy groups have been successfully self-assembled to the microstructure surface, reducing the microstructure surface free energy to obtain a superhydrophobic surface.

The key factor in preparing SHP surfaces is to establish a rough surface morphology surface. Fig. 3 shows the surface morphology of aluminum alloy after different spraying time modification by SEM scanning microscope. It can be seen that the surface of unmodified aluminum alloy, with a smooth surface structure and only some regular protrusions and grooves from Fig. 3(a). With the change of different spraying time, Fig. 3(b) shows the surface morphology of 5 s is relatively flat which can't form a structure. It is observed from Fig. 3(c) and (d) that the particles on the surface gradually agglomerate and adhere to the aluminum surface to form a rough microstructure like peak structure which built up by the spraying pressure that begin to appear on 10 s and 15 s. Fig. 3(e) shows the increase of spraying time leads to the gradual formation of particle agglomeration on the surface from flat, which is mainly attributed to the existence of fluorinated SiO_2 particles on the
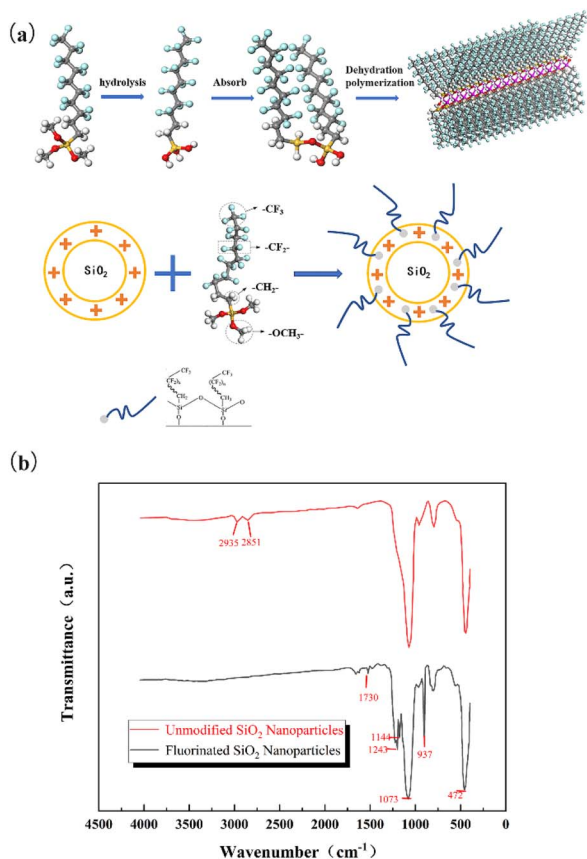

Fig. 2 (a) Formation mechanism of modified SiO_2 nanoparticles on the surface; (b) FTIR diagram of unmodified SiO_2 nanoparticles and fluorinated SiO_2 nanoparticles. Analysis of surface morphology of spraying time.
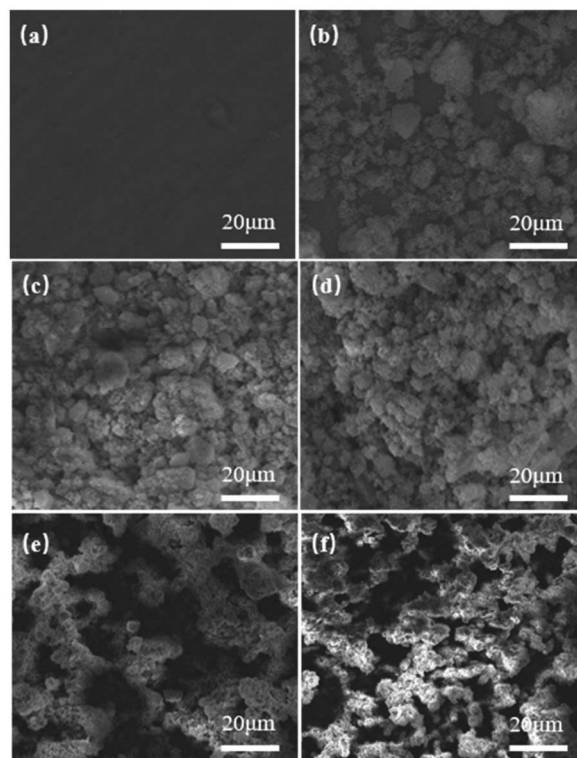

Fig. 3 SEM images of SHP surface morphology with different spraying time: (a)SHP-0; (b) SHP-5; (c) SHP-10; (d) SHP-15; (e) SHP-20; (f) SHP-25.

surface, and EP and PAI are easy to agglomerate to form obvious micro–nano structure. When the coating spraying time at 25 s, the excessively thick micro nano structure will cover micro–nano structure and the increase of solid–liquid area.

Analysis of surface wettability of spraying time

The preliminary wettability and adhesion behaviors of SHPs were tested by the water contact angle (WCA) and sliding angle (SA), respectively. SiO_2 nanoparticles are hydrophilic inherently, after the fluorination reaction, the coating surface has certain different hydrophobicity by adjusting the spraying time. With the increase of spraying time between 0 s and 25 s, SHP with different surface morphology enables the interaction between the surface and water droplets differently. A trend of WCA shows increases first and then decreases at a small range in Fig. 4. The WCA of the surface is less than 150° while the spraying time is less than 10 s, which means that changing the spraying time can adjust the WCA of the surface. Similarly, when the spraying time is 20 s, the hydrophobicity of the surface is 160.4° ± 1.3° which repels the water excellently. When the spraying time continues to increase, the hydrophobicity of the surface begins to decline which can be attributed to the following two reasons. On the one hand, the reason is related to the unstable surface morphology and leads to a large error in the surface wettability test results when the surface coating is too thick. On the other hand, if the coating thickness continues to increase, the internal stress may be larger, that causing cracks on the coating surface. Sliding angle explains the behavior of surface adhesion. Water droplets adhere to the surface (from 23.1° ± 1.5° to 12.0° ± 3.1°) while the spraying time is less than 10 s. With the spraying time reaching 20 s, the adhesion of the surface reaches the minimum which the sliding angle is 4.1° ± 1.0°. The phenomena indicates that the wetting state between SHPs and water droplets varied from spraying time.

Surface roughness and wetting model spraying time of the coating

To better understand the effect of spraying time on the surface coating, understand the surface morphology and the change
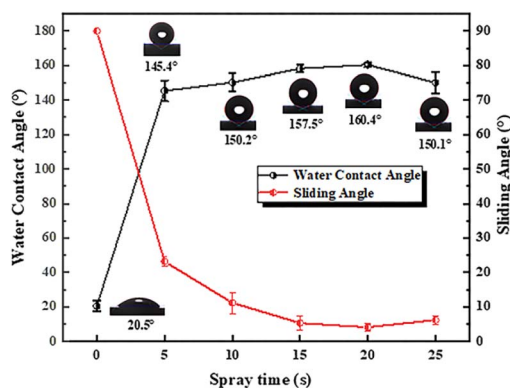

Fig. 4 The WCA and SA different spraying time of SHPs coatings with different spraying time.

law of surface wettability, we characterized the surface morphology and roughness parameters of SHPs with Ultra-Depth 3D Microscope in Fig. 5(a)–(g). It can be seen that with the change in spraying time, the 3D morphology formed on the surface and roughness has an obvious difference. When the spraying time is only 5 s, the structure height on the surface is 5 μm, as the spraying time increases to 10 s and 15 s, the coating height increases by 21 μm and 40 μm, and a stable cluster structure is formed on the surface and the height reaches 60 μm, and when the spraying time is 25 s, the coating height changes to 98 μm. The coating height changes greatly, which is due to the destruction of the structure formed during the spraying process and the aggregation of a large number of micro and nanoparticles, and the poor mechanical properties of the coating formed by the aggregation of these particles. The changes in surface morphology affect the wettability change behaviors of the surfaces as shown in Fig. 5(g). When the spraying time exceeds 5 s, the rough structure formed on the surface can obtain a larger solid–liquid contact area, which makes the surface wetting state from Wenzel state to Cassis–Baxter state.[31] The Laplace pressure formed in the rough structure of the surface is not enough to support the droplets to completely suspend on the fluorinated SiO_2 molecular surface, resulting in the formation of Wenzel state on the surface as the spraying time is less than 5 s. The experimental results show that the rough structure formed on the surface can directly support the water droplets leading to the Cassis–Baxter state of spraying time was 20 s, and with the increase of time, the gap will be filled with excess particles.

Simultaneously, the changing trend of roughness is consistent with that of line profile as shown in Fig. 6, and with the change of spraying time, the roughness R_a changes from 0.056 μm to 6.627 μm, the roughness R_q changes from 0.073 μm to 7.292 μm. The results show that with the change in spraying time, the surface morphology forms peaks and troughs with different spacing, and the corresponding air supported droplets captured in the troughs can be suspended on the coating surface.

Analysis of anti-icing performance of the coating

For its surface structure of coating modification, super-hydrophobic surfaces, with excellent anti-icing properties, have a bright future in anti-icing applications. The reason why superhydrophobic surfaces have good anti-icing performance is the existence of a micro–nano structure, that makes the surface in the Cassie–Baxter state and thermal conductivity, water droplets can be suspended over the superhydrophobic surfaces and easily roll off.[32] As discussed above, the static water droplet icing change of SHPs coating was tested to reflect their anti-icing performance. The process of ice formation is mainly divided into the pre-cooling stage and the nucleation and growth stage of droplets. Fig. 7 shows the real-time status of the water droplet of 5 μL on the prepared surface of SHPs with different spraying time. Compared with the pre-cooling time (before ice nucleation), the time of ice growth is significantly shorter, once nucleation occurs, the ice will move from the
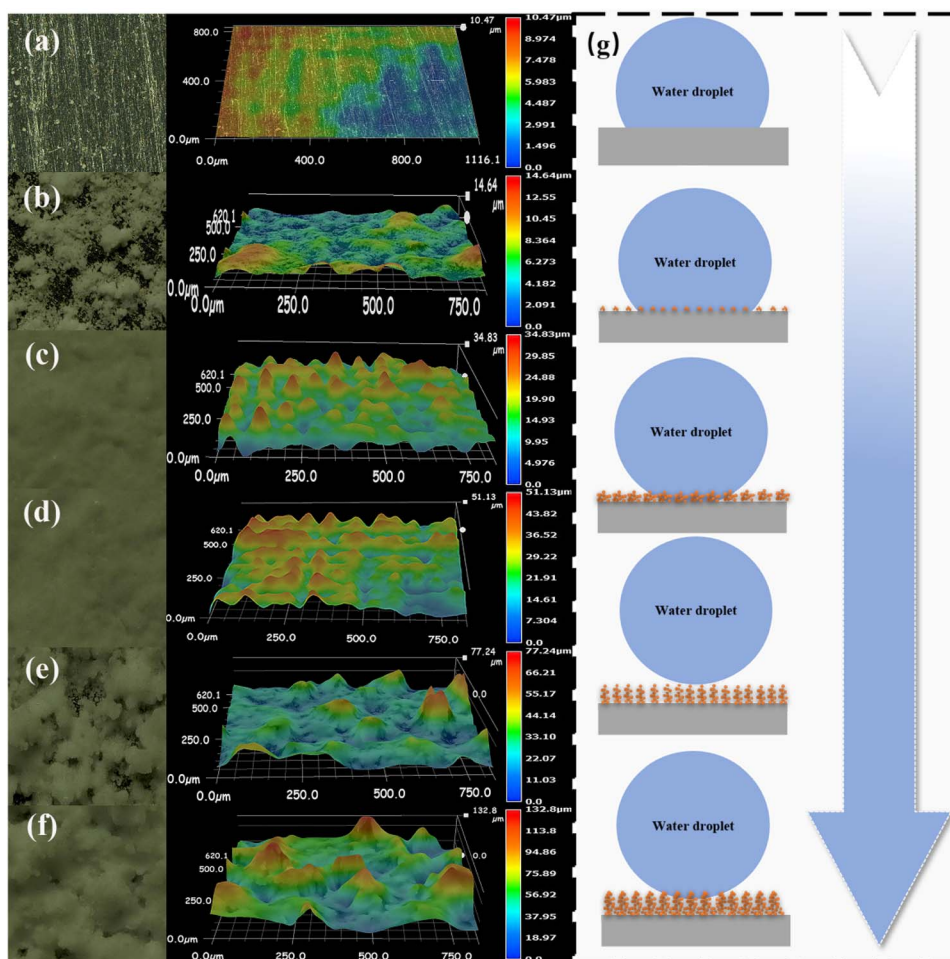
Fig. 5 3D surface images of SHP with different spraying time (a) SHP-0; (b) SHP-5; (c) SHP-10; (d) SHP-15; (e) SHP-20; (f) SHP-25; (g) the schematic of the wetting model of SHP with different spraying time.
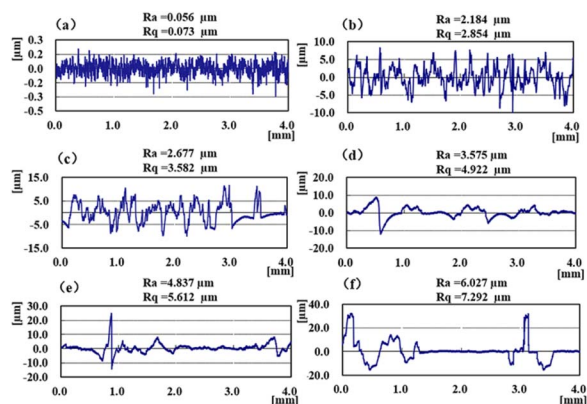

Fig. 6 Surface roughness of SHP with different spraying time: (a) SHP-0; (b) SHP-5; (c) SHP-10; (d) SHP-15; (e) SHP-20; (f) SHP-25.

Fig. 7 (a) Freezing process (−15 °C) of droplets on SHPs with different spraying time: (a1) SHP-0; (a2) SHP-5; (a3) SHP-10; (a4) SHP-15; (a5) SHP-20; (a6) SHP-25; (b) icing mechanism of coating surface; (c) the heat transfer process of coating.

bottom to the upper liquid phase. Fig. 7(a1) shows bare aluminum surface and SHPs coating surface central area are transparent. With the progress of the experiment, the surface temperature decreased gradually, the central area of drops became non-transparent at first after 32 s, and the water
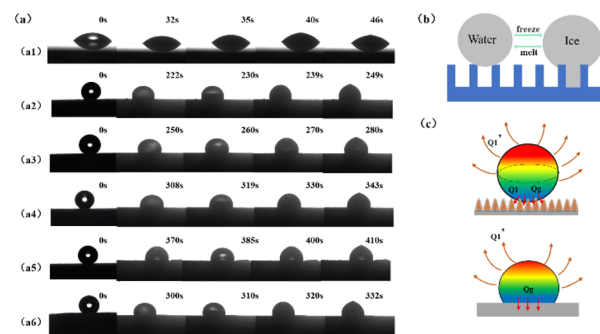
droplets on the surface quickly freeze for about 14 s. It is worth noting that the drop on the SHP-20 conforms to Cassie–Baxter wetting model becomes non-transparent after 370 s, and the water droplets on the surface freeze for about 40 s, the pre-cooling time of surface droplet icing accounts for about 90% of

the total ice delay time. Moreover, Fig. 7(a1)–(a6) shows the state of frozen droplets on different wettability surfaces, and with the increasing of spraying time, the freezing time of SHPs increased first and then decreases which is consistent with the change trend of wettability.

To further explain the process of the change of the wettability of the droplet icing, Fig. 7(b) shows the mechanism of the change of the freezing process of the superhydrophobic surface. When the temperature of the experimental plate is maintained at −15 °C and the ambient humidity is 50 ± 5 wt%, the Cassie–Baxter state still exists on the SHP when the freezing behavior occurs. With the progress of time, the wettability of the surface begins to decline, due to the air trapped on the hydrophobic surface condensing, and the droplets are not suspended on the surface at all. At this time, the surface is in Wenzel state. Surprisingly, when the surface coating restores at the ambient temperature, SHP regains its superhydrophobic property. The reason is the internal water vapor in the air melted and the droplets were suspended by the surface structure. It can be seen from Fig. 8 that the wettability of the droplets decreases significantly during the precooling process and the freezing process. After drying at a high temperature of 50 °C, the water contact angle of the coating surface decreases, but the decrease is not obvious. It is further proved that the mechanism of the droplet icing process is that the water vapor in the internal air condenses to form Wenzel state, which can still be restored after melting.

The coating can improve the thermal resistance of the heat transfer process and delay the icing process. It is assumed that the droplet is always spherical and the heat transfer between the droplet and air is uniform. From Fig. 7(c), shows the heat transfer process of coating surface and smooth surface. According to the heat conduction formula:

$$Q = Q_g + Q_l + Q_l' \tag{1}$$

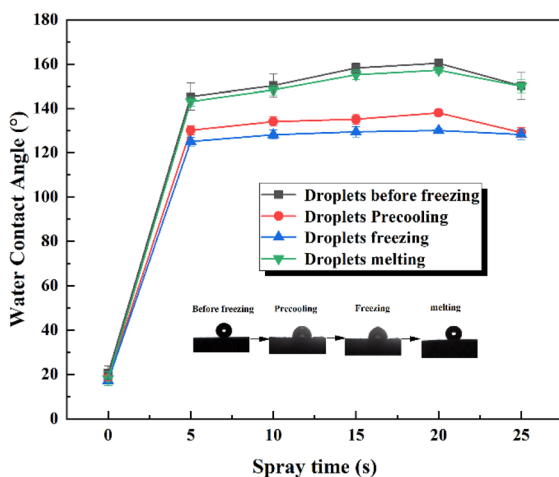Q is heat transfer during the whole icing process; Q_g is heat transfer in heat conduction process; Q_l is heat transfer in natural convection process. Q_l' is heat transfer in thermal radiation process.

Based on Fourier's law, Newton's cooling law and Stephen Boltzmann's law, the heat transfer process equation can be described as:

$$Q_g = \alpha 2\pi R^2 (1 + \sin\theta)(T_d - T_s)$$
$$+ C_n 2\pi R^2 (1 - \sin\theta)(T_d^* - T_s) + Q_l' \tag{2}$$

α is the silica thermal conductivity is 0.27 W cm^{-1} K^{-1},[33] R is the droplet radius, θ is contact angle of coating surface T_d is the ambient temperature, T_d^* is the temperature of trapped air T_s is the droplet temperature.

There is no air is trapped on the smooth surface, and the solid–liquid contact area is much larger than the superhydrophobic surface. The heat transfer process on the surface can be described as follows:

$$Q_s = Q_g + Q_l' = \alpha_1 2\pi R^2 (1 + \sin\theta)(T_d - T_s) + Q_l' \tag{3}$$

α_1 the thermal conductivity of aluminum is 237 W cm^{-1} K^{-1}.[34] According to the literature,[35] it is proved that the heat transfer between liquid–solid interfaces is the main form of droplet heat loss. It can be inferred that the low thermal conductivity and high wettability of the droplets on the coating surface are the main factors for the delayed icing of the droplets on the surface.

To discuss the influence of the droplet icing delay performance accurately, the droplet icing delay performance was also characterized at −9 °C, −12 °C, −15 °C, and −18 °C, as shown in Fig. 9(a) and (b). With the decrease of substrate temperature, the anti-icing ability of static droplets on SHPs surface decreases rapidly, the precooling time and the ice growing time of water drops on different SHPs surfaces reducing greatly while the substrate temperature is −9 °C and −18 °C. And it can be found that at lower temperatures, the droplet icing delay time of the superhydrophobic surface of the micro–nano composite structure is still significantly improved compared with the SHP-0, and still shows a higher icing delay performance.

Coating durability and wear resistance test

Durability of the SHP-20 was evaluated by exposing it to the air for 180 days.[36] Fig. 10(b) shows the WCA and SA slightly changed by less than 7.0° ± 3.4° during air exposure for 6

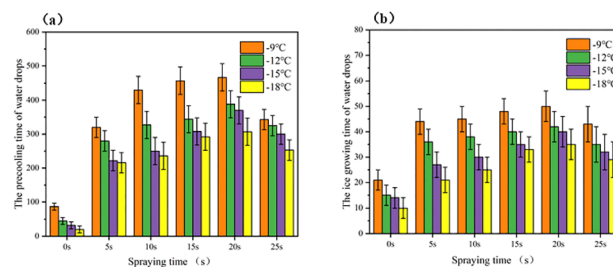Fig. 8　Change of water contact angle during droplet freezing and melting at different spraying time.

Fig. 9　(a) The pre-cooling time of water droplets on −9 °C, −12 °C, −15 °C, and −18 °C with different spraying time; (b) the growing time on −9 °C, −12 °C, −15 °C, and −18 °C with different spraying time.
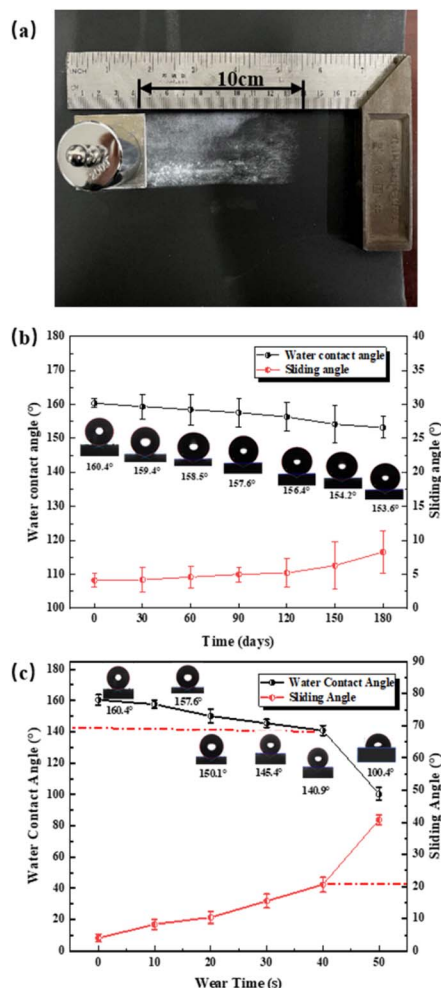
Fig. 10 (a) Abrasion resistance test of SHP-20 specific wearing steps; (b) water contact angles and sliding angles of SHP-20 exposed to the air for 180 days; (c) results of SHP-20 after 50 times of sandpaper friction cycle test.

months, which indicates that the SHP-20 coating has long-term stability in the air. On the other hand, to test the wear resistance of the superhydrophobic coating, 50 sandpaper friction cycle tests were carried out according to the scheme of ref. 37 and 38. Fig. 10(a) shows the water contact angle of the coating was tested respectively, and Fig. 9(b) shows the specific steps. It can be seen from Fig. 10(c) that after 40 times sandpaper friction cycle test, the WCA can maintain above $140.9° \pm 1.8°$ and the SA change to $21° \pm 2.1°$, indicating that the coating has possessed good abrasion resistance.

Conclusions

We have fabricated a super hydrophobic aluminum surface in which SiO_2 nanoparticles and HFTMS combine to form low surface energy substance and mixed with EP and PAI by one-step spraying method by adjusting spraying time. Our results show the performance of the coating with different spraying time changes in surface morphology and surface roughness, SHP-20 shows the highest water contact angle of $160.4° \pm 1.3°$

and a sliding angle of $4.1° \pm 1.0°$. Due to their different wettability, we designed experiments and proved that the coatings have anti-icing performance with different wettability at -15 °C by simplifying the theory heat conduction. At the same time, the lower surface temperature can greatly short the icing time. The SHP-20 surface coating also shows good mechanical properties and durability performance. This study provides a low cost produced method to study the influence of surface morphology on wettability and anti-icing properties for various applications.

Author contributions

Jun Xie performed experiments, analysed the results and wrote the paper. Xiaoru Hao supervised the study, arranged funds and finalized the article. Yu Zhang provided experimental help and paper modification suggestions. Zhihao Cheng provided experimental help. Wei Sheng arranged experiment equipment and finalized the article.

Conflicts of interest

The authors declare that they have no known competing financial interests or personal relationships that could have appeared to influence the work reported in this paper.

Acknowledgements

Notes and references

1 J. Han, M. Cai, Y. Lin, W. Liu, X. Luo, H. Zhang, K. Wang and M. Zhong, *RSC Adv.*, 2018, **8**, 6733–6744.
2 Y. Wang, L. Guan, Z. He, J. Tan, H. Singh, M. D. Hayat and C. Yao, *Surf. Eng.*, 2021, **37**, 1246–1254.
3 G. Wang, Y. Shen, J. Tao, X. Luo, L. Zhang and Y. Xia, *RSC Adv.*, 2017, **7**, 9981–9988.
4 Y. Shen, S. Liu, C. Zhu, J. Tao and G. Wang, *Chem. Eng. J.*, 2017, **313**, 47–55.
5 T. Nishino, M. Meguro, K. Nakamae, M. Matsushita and Y. Ueda, *Langmuir*, 1999, **15**, 4321–4323.
6 B. J. Basu, T. Bharathidasan and C. Anandan, *Surf. Innovations*, 2013, **1**, 40–51.
7 S. Taheri, F. H. Motlagh, S. Dehestanizad, H. Yahyaei, A. Motallebzadeh, A. Zarrabi, A. G. Tehrani, M. Khodabakhsh and H. Makki, *Surf. Interfaces*, 2022, **30**, 101824.
8 P. Rodič and I. Milošev, *Surf. Coat. Technol.*, 2019, **369**, 175–185.
9 H. Ogihara, T. Katayama and T. Saji, *J. Colloid Interface Sci.*, 2011, **362**, 560–566.
10 H. Kim, K. Nam and D. Y. Lee, *Polymers*, 2020, **12**, 1420.
11 H. Zheng, W. Liu, S. He, R. Wang, J. Zhu, X. Guo, N. Liu, R. Guo and Z. Mo, *Colloids Surf., A*, 2022, **648**, 129152.

12 P. Wang, T. Yao, B. Sun, X. Fan, S. Dong, Y. Bai and Y. Shi, *Colloids Surf., A*, 2017, **513**, 396–401.

13 N. Chi-Vinh and C. Doo-Man, *CIRP Ann.-Manuf. Technol.*, 2018, **67**, 571–574.

14 Y. Shu, X. Lu, Y. Liang, W. Su, W. Gao, J. Yao, Z. Niu, Y. Lin and Y. Xie, *Surf. Coat. Technol.*, 2022, **441**, 128514.

15 Z. Qin, J. Ai, Q. Du, J. Liu and X. Zeng, *Mater. Des.*, 2019, **173**, 107782.

16 N. Ma, D. Cheng, J. Zhang, S. Zhao and Y. Lu, *Surf. Coat. Technol.*, 2020, **399**, 126180.

17 K. Nakayama, T. Hiraga, C. Zhu, E. Tsuji, Y. Aoki and H. Habazaki, *Appl. Surf. Sci.*, 2017, **423**, 968–976.

18 H. Kang, B. Zhao, L. Li and J. Zhang, *J. Colloid Interface Sci.*, 2019, **544**, 257–265.

19 Y. Wang, Y. Liu, L. Zhang, M. Zhang, G. He and Z. Sun, *Appl. Surf. Sci.*, 2019, **496**, 143743.

20 A. Accardo, F. Di Stasio, M. Burghammer, C. Riekel and R. Krahne, *Part. Part. Syst. Charact.*, 2015, **32**, 524–528.

21 X. Cao, Q. Ding, A. Gao, H. Lv, N. Zhao and D. Liu, *J. Colloid Interface Sci.*, 2017, **494**, 170–177.

22 T. P. Manoj, T. P. Rasitha, S. C. Vanithakumari, B. Anandkumar, R. P. George and J. Philip, *Appl. Surf. Sci.*, 2020, **512**, 145636.

23 A. Gaddam, H. Sharma, R. Ahuja, S. Dimov, S. Joshi and A. Agrawal, *Microfluid. Nanofluid.*, 2021, **25**, 9.

24 Z. Zhao, H. Chen, X. Liu, Z. Wang, Y. Zhu and Y. Zhou, *Surf. Coat. Technol.*, 2020, **404**, 126489.

25 N. Valipour Motlagh, J. Sargolzaei and N. Shahtahmassebi, *Surf. Coat. Technol.*, 2013, **235**, 241–249.

26 W. Guo, C. Liu, N. Li, M. Xi, Y. Che, C. Jiang, S. Zhang and Z. Wang, *Nanoscale Adv.*, 2022, **4**, 2884–2892.

27 S. Jung, M. Dorrestijn, D. Raps, A. Das, C. M. Megaridis and D. Poulikakos, *Langmuir*, 2011, **27**, 3059–3066.

28 X. Wu, X. Zhao, J. W. C. Ho and Z. Chen, *Chem. Eng. J.*, 2019, **355**, 901–909.

29 Y. Hou and K. L. Choy, *Prog. Org. Coat.*, 2022, **163**, 106637.

30 R. Zhang, P. Hao, X. Zhang and F. He, *Int. J. Heat Mass Transfer*, 2018, **122**, 395–402.

31 D. Murakami, H. Jinnai and A. Takahara, *Langmuir*, 2014, **30**, 2061–2067.

32 D. Yue, S. Lin, M. Cao, W. Lin and X. Zhang, *Cellulose*, 2021, **28**, 3745–3758.

33 W. Chen, Y. Feng, L. Qiu and X. Zhang, *Int. J. Heat Mass Transfer*, 2020, **154**, 119750.

34 H. Pan, F. Pan, R. Yang, J. Peng, A. Tang, Q. Huang, K. Song and Z. Gao, *Int. J. Heat Mass Transfer*, 2014, **30**, 988–994.

35 X. Li, G. Wang, A. S. Moita, C. Zhang, S. Wang and Y. Liu, *Appl. Surf. Sci.*, 2020, **505**, 144386.

36 Y. Gao, Y. Sun and D. Guo, *Appl. Surf. Sci.*, 2014, **314**, 754–759.

37 I. Torun and M. S. Onses, *Surf. Coat. Technol.*, 2017, **319**, 301–308.

38 M. Mokter Hossain, Q. H. Trinh, M. S. P. Sudhakaran, L. Sultana and Y. S. Mok, *Surf. Coat. Technol.*, 2019, **376**, 124785.